On the absence of asymmetric wakes for periodically plunging finite wings

D. E. Calderon, D. J. Cleaver, I. Gursul, and Z. Wang

Citation: Physics of Fluids (1994-present) **26**, 071907 (2014); doi: 10.1063/1.4891256
View online: http://dx.doi.org/10.1063/1.4891256
View Table of Contents: http://scitation.aip.org/content/aip/journal/pof2/26/7?ver=pdfcov
Published by the AIP Publishing

PHYSICS OF FLUIDS **26**, 071907 (2014)

On the absence of asymmetric wakes for periodically plunging finite wings

D. E. Calderon, D. J. Cleaver, I. Gursul, and Z. Wang
Department of Mechanical Engineering, University of Bath, Bath BA2 7AY, United Kingdom

(Received 14 March 2014; accepted 14 July 2014; published online 31 July 2014)

It has previously been shown that, at high Strouhal numbers, oscillating airfoils can produce deflected jets that can create very high lift-coefficients for otherwise symmetric scenarios. These deflected jets form through pairing of the trailing-edge vortices to create asymmetric vortex couples that self-propel at an angle to the freestream, resulting in an asymmetric flow field and non-zero lift. In this paper results are presented that indicate these high-lift deflected jets cannot form for finite wings. Instead of the straight vortex tubes that pair and convect at an angle to the freestream observed for effectively infinite wings, finite wings exhibit vortex tubes that break into two branches near the tip forming double helix structures. One branch connects with the last vortex; one branch connects with the next vortex. This creates a long "daisy chain" of interconnected trailing edge vortices forming a long series of vortex loops. These symmetric flow fields are shown to persist for finite wings even to Strouhal numbers more than twice those required to produce asymmetric wakes on plunging airfoils. Two contributing reasons are discussed for why deflected jets are not observed. First the tip vortex creates three-dimensionality that discourages vortex coupling. Second, the symmetry of the circulation of the interconnected vortex loops, which has been confirmed by the experiments, is a natural consequence of the vortex topology. Therefore, the asymmetry in trailing edge vortex strength previously observed as characteristic of deflected jets cannot be supported for finite wings. [http://dx.doi.org/10.1063/1.4891256]

I. INTRODUCTION

Flapping wings are the preferred method of natural propulsion both through the air and through water. Birds, insects, and fish commonly employ wing oscillations as a means of lift and/or thrust generation with the kinematic motion altered to evoke different manoeuvres, for example, to loiter or propel themselves forward. The fluid dynamics that govern these flows are of fundamental interest and have become more important recently due to the growing desire to develop efficient Micro Air Vehicles (MAVs). Improved understanding of these unsteady flows, and in particular the vortex shedding mechanisms,[1] is necessary if man-made flyers hope to achieve similar performance at small scales. Natural flyers use a large-amplitude low-frequency (low Strouhal number) flapping motion. In this paper, we consider the opposite: small-amplitude high-frequency (high Strouhal number) motion. The only commonality with nature is the generation of leading-edge and trailing-edge vortices. The kinematics in our case is relevant to the exploitation of aeroelastic vibrations for flow control purposes, through excitation by wing oscillations. In fact, our approach is a flow control method to increase lift, and is only applicable to small aircraft because the frequencies of the wing structure can provide sufficiently high Strouhal numbers.[2] We study rigid airfoils and wings in small-amplitude forced plunging motion, which mimics bending oscillations. In our previous work we identified a mechanism of high-lift production due to the bifurcated/asymmetric flows. These deflected wakes can lead to time-averaged lift coefficients higher than any other mechanism.

An important parameter used in the study of plunging wings is the Strouhal number based on the amplitude, $St_A = 2fa/U_\infty$, where f is the plunge frequency, $2a$ is the peak-to-peak amplitude,

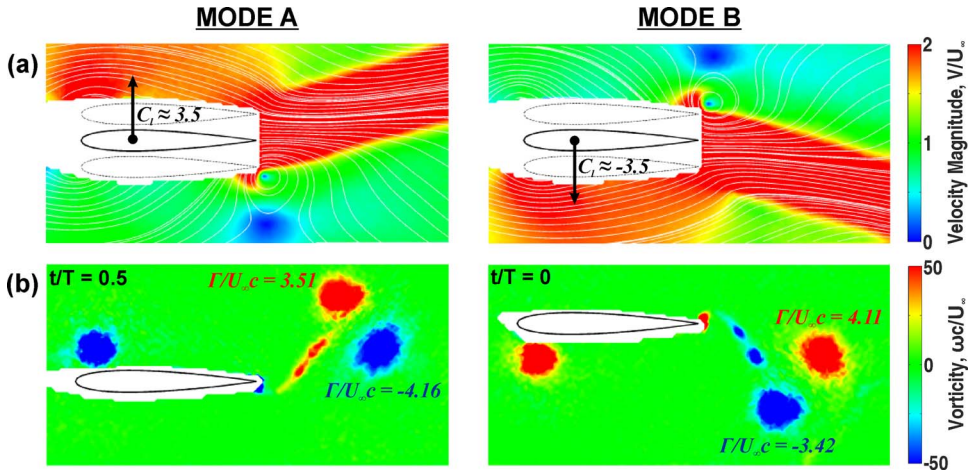

FIG. 1. (a) Time-averaged velocity showing deflected jets for a NACA0012 airfoil at $\alpha = 0°$ and Re = 10 000. The direction of the deflected jet determines the positive or negative lift coefficient and is characterised by asymmetry in the trailing-edge vortex strength; (b) phase-averaged vorticity (adapted from Cleaver *et al.*[8]). Reprinted with permission from Cleaver *et al.*, J. Fluid Mech. **708**, 349–376 (2012). Copyright 2012 Cambridge University Press.

and U_∞ is the freestream velocity. It is a dimensionless parameter that describes the ratio between plunging and freestream velocity. An increase in Strouhal number results in a monotonic rise in effective angle of attack because it depends on the term: $\tan^{-1}(U_{pl}/U_\infty)$ where the maximum plunge velocity is $U_{pl} = 2\pi fa$. The ability of an oscillating wing to generate thrust is a well-established phenomenon. A parameter space consisting of flapping amplitude, $2a$, and the Strouhal number St_A, is often considered in order to characterise the wake vortex patterns. However, there is also a strong influence of the non-dimensional frequency, $St_c = fc/U_\infty$, (where c is the chord length), when there is separation and a leading-edge vortex. Studies have found that at a sufficient combination of the amplitude and frequency, a switch occurs in the wake vortex pattern. The staggered array of vortices that are characteristic of bluff body wakes invert their positions to form a reverse von Kármán Street.[3] Therefore, if the flow is from left to right, the counter clockwise vortices move above the horizontal line, while the clockwise vortices move below. The wake deficit is therefore replaced with a wake surplus resulting in a jet in the time-averaged flow that is indicative of thrust.

At even higher Strouhal numbers studies have shown that the clockwise and counter-clockwise trailing edge vortices may begin to shed in pairs and propagate at an angle to the streamwise axis; thereby describing a form of asymmetric shedding even for zero angle of attack. An example is shown in Figure 1. This symmetry breaking process was first observed by Bratt[4] but remained largely unnoticed until Jones *et al.*[5] used an unsteady inviscid panel code, and simulated deflected jets on a plunging two-dimensional airfoil. The formation of deflected jets was therefore deemed an inviscid phenomenon and leading edge separation was not considered a prerequisite for its inception. In these computations, once formed, the direction of the deflected jet was constant, and could therefore be described as stable. It is largely recognised that for these stable deflected jets the initial choice of jet direction, up or down, is determined by the initial conditions,[6–8] i.e., the starting position and acceleration time. Godoy-Diana *et al.*[6] explain that the initial trailing edge vortex entrains fluid from behind, thereby deflecting the mean flow which results in a change in the vortex couple trajectory. Similarly Cleaver *et al.*[8] showed that the choice of mode is determined by the interaction of the vortices from the first two cycles and that this is a very complex process which will depend on multiple parameters. However, in these studies once established this direction does not change.

Conversely, the water tunnel experiments of Jones *et al.*[5] revealed that the direction of these deflected vortex couples may somewhat randomly switch between an upward or downward "mode" and can therefore be described as unstable in some cases. This instability was not observed in their inviscid panel method. The viscous solution of Lewin and Haj-Hariri[9] successfully simulated similar switching for a similar plunging NACA0012 airfoil, implying that the switch may be driven

by disturbances from the leading edge separation. Experimentally Heathcote and Gursul[10] showed that switching may occur periodically over a continuous series of cycles with a period on the order of one hundred plunging period. Likewise Cleaver *et al.*[11] observed a very similar jet switching period of around one hundred plunging period for a flat-plate airfoil. In this case the geometry was shown to be crucial, with a NACA 0012 geometry stable deflected jets occur whereas with a flat-plate geometry unstable deflected jets occur. All of these results would indicate that it is the leading-edge separation which drives the jet switching phenomenon but deflected jets can exist without leading-edge separation, i.e., their formation is associated with the behaviour of the trailing-edge vortices (TEVs).

It was shown that dual flow fields (two possible deflection angles of the jet) exist even at non-zero angles of attack up to the stall angle.[8] Observations indicate that deflected jets form once the TEVs reach sufficient strength at high Strouhal numbers. Several studies[5,6,8,12–14] reported critical Strouhal number in the range of $St_A = 0.32$–0.45. Critical strength[8] was reported as $\overline{|\Gamma|}/U_\infty c = 2.6$ or $\overline{|\Gamma|}/U_{pl}c = 1.85$, where Γ is the circulation of the trailing-edge vortices. The first two criteria, St_A and $\Gamma/U_\infty c$, cannot be considered universal criteria due to the wide scatter in results both across different studies and systematic variation within individual studies. The third criterion shows more promise but needs further validation. Similarly Godoy-Diana *et al.*[14] consider a condition for TEV asymmetry on a pitching two-dimensional airfoil, based on the magnitude and direction of the self-induced velocity of a vortex couple, and its horizontal advection speed relative to the freestream velocity. The "effective phase velocity" of the vortex couple defines a parameter in which a positive value describes a satisfactory condition for deflected jets to occur.

In terms of what characterizes the direction of the deflected jets Cleaver *et al.*[8] propose that the angular velocity of a vortex couple can be used to define the mode choice. For example, Figure 1 shows a stable upwards deflected jet (Mode A – left) and downwards deflected jet (Mode B – right). For the upwards deflected jet the counter-clockwise TEV is the stronger of the two; whereas in the case of the downward deflected jet the clockwise TEV is the stronger of the two. This asymmetry in the TEV strength describes the direction of the deflected jet and was observed for all cases studied across a range of amplitudes and mean angles of attack. It also explains why dual flow fields are not observed for larger angles of attack (the angle of attack creates a natural bias in the TEV strength towards a mode B flow field).

Naturally these time-averaged jets and the choice of mode have been shown to have significant influence on lift. Cleaver *et al.*[8] showed that for zero mean angle of attack, an upward deflected jet is associated with significant positive lift: $C_L \sim 3.5$, whilst a downward deflected jet results in the opposite, significant negative lift: $C_L \sim -3.5$. Similar observations were made by Yu *et al.*[15] As deflected jets occur at values of St_A similar to natural flyers there is a possibility that the phenomenon is exploited as a means of lift augmentation in natural flight.[6] However, similar asymmetric wakes have not been observed for finite wings, which raises the question whether this phenomenon is even possible in the three-dimensional flows produced by finite wings. Instead of distinct two-dimensional vortices finite wings exhibit continuous chains of interconnected vortex loops.[16–21] As the Strouhal number is increased beyond about $St_A = 0.35$, two oblique jets that are *symmetric* develop as a result of two branches of distinct interconnected vortex loops. This symmetric time-averaged wake is different than the asymmetric wakes for two-dimensional airfoils shown in Figure 1.

In this paper we demonstrate that deflected jets do not occur, in the wide range of parameters studied, for finite wings through direct comparison of an effectively infinite wing and finite wing cases at the same experimental parameters with the same experimental setup. We then present detailed flow field measurements for a typical case and suggest two mechanisms that contribute to the absence of deflected jets in finite wing cases.

II. EXPERIMENTAL METHODS

A. Experimental setup

The experiments were performed in a water tunnel at the University of Bath. The Eidetics® Model 1520 consists of a free-surface closed-loop system capable of flow speeds of up to 0.5 ms^{-1}.

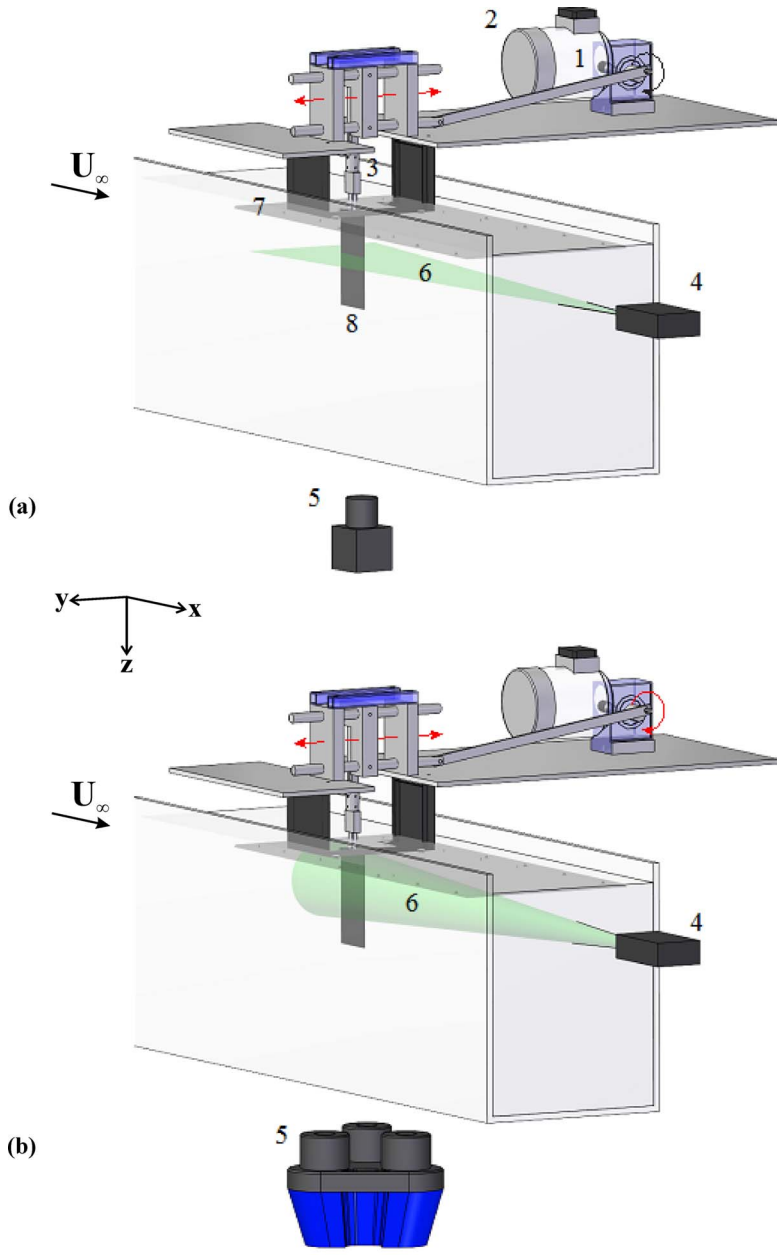

FIG. 2. Experimental setup and apparatus for the (a) PIV and (b) volumetric velocimetry system. 1: rotary encoder, 2: motor, 3: force balance, 4: laser, 5: camera, 6: laser sheet/cone, 7: end plate, 8: wing.

The test section is 1520 mm long, 381 mm wide, and 508 mm deep, providing optical access from beneath, the sides and through a downstream viewing window. A series of honeycomb structures, located upstream of the test section ensure a turbulence intensity of less than 0.5%.

The experimental rig is placed on top of the test section and drives the vertically mounted, fully submerged wing in lateral oscillations across the width of the tunnel, see Figure 2. The wing oscillations are made possible via a crank arm mechanism, powered by an AC 0.37 kW Motovario three-phase motor with a 5:1 gearbox reduction ratio. The crank arm was designed to be long enough, relative to the turning radius, to ensure that the wing displacement was sufficiently close to that of a sinusoidal curve. Trailing edge tracking was used to verify that the actual displacement is within 1.25% of the peak-to-peak amplitude of the required sine curve. The motor spin rate and therefore,

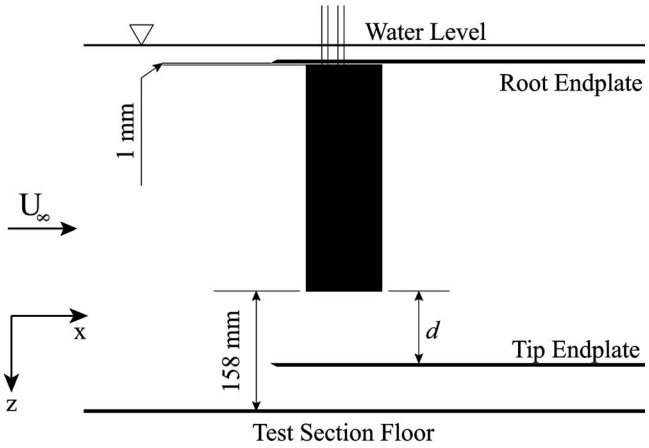

FIG. 3. A schematic of the test section, showing the $b/c = 3$ rectangular wing. The distance d between the tip of the wing and the endplate is varied by adjusting the height of the tip endplate, from the base of the test section.

plunging frequency is regulated with an IMO Jaguar Controller and the amplitude is set prior to the start of the tests and simply defined by the crank arm turning radius. The geometric angle of attack is also kept constant at $\alpha = 0^\circ$ throughout the oscillation to impose a pure plunging motion. For the majority of the cases studied, Reynolds number is $Re = 1 \times 10^4$ and the amplitude of the plunging motion was set to $a = 0.15c$ with the forcing frequency varied in the range $St_c = 0$–2.025, corresponding to a reduced frequency of $k = \pi fc/U_\infty = 0$–6.36. For the lower Reynolds cases, $Re = 0.5 \times 10^4$, the amplitude was still $a = 0.15c$ but the forcing frequency varied in the range $St_c = 0$–4.050.

The wing has a NACA 0012 cross section, rectangular planform, and a span of $b/c = 3$. In order to remove free surface effects, an end-plate was placed below the free surface, at the root of the wing, yielding a half-model. For the two-dimensional airfoil cases a further end-plate was placed at the tip of the wing to create an effectively infinite wing (not shown in Figure 2). The maximum blockage ratio was 3.1%. To investigate the effect of tip spacing (d) and the transition from effectively infinite to finite wing, this end-plate was adjustable so that the height of the tip endplate from the base of the water tunnel test section could be increased/decreased, see Figure 3.

B. Techniques

1. Force measurements

Force measurements were performed using a two-component binocular strain-gauge balance. Two sets of four bonded strain gauges were connected to form two Wheatstone bridges with an excitation voltage of ±6.5 V. Signal conditioning was applied using an input instrumentation AD624 amplifier, allowing the signal to be zeroed, amplified and filtered at different stages. The conditioning card provides two gain stages. The input stage has a maximum gain of 500, and the output stage has a finely adjustable gain of 5.54–10.9. A two-pole low pass Butterworth filter was set to 30 Hz. Finally, an AD/DA converter prepares the signals for the data acquisition card before being monitored and stored using an in-house LabView program.

A total of 30 000 data points at a sampling rate of 360 per oscillation cycle were averaged to generate a mean lift coefficient for a single frequency. This was repeated for various frequencies. It is important to note that within the instantaneous signal there exists an inertia component. The average of this inertia force over a complete number of cycles is zero, allowing us to time-average the instantaneous force to obtain the time-averaged lift force. The uncertainty associated with these time-averaged lift measurements increases with increasing frequency. For a typical case the uncertainty of the time-averaged lift coefficient increases from ±0.03 at $St_c = 0$, to ±0.35 at $St_c = 2.025$.

2. Particle image velocimetry

A series of flow field measurements were taken with a Particle Image Velocimetry (PIV) system. The TSI Inc. 2D-PIV system comprises of a dual ND:YAG 50 mJ pulsed laser, illuminating the streamwise plane. The flow was seeded with 8–12 μm hollow glass particles and the illuminated plane was then captured by a 2MP Powerview Plus 12bit CCD camera. The positioning of the camera and the laser sheet with respect to the test section is illustrated in Figure 2. The end-plate used for the effectively infinite wing, which is not shown in Figure 2, is transparent to allow optical access. A rotary encoder fitted to the worm gear spindle produced 360 pulses per cycle, each within equal time intervals. Combined with an in-house pulse selection system and a LaserPulse synchroniser this allowed the laser to be fired at any desired phase in the cycle. The pair of laser sheets were fired approximately 750 μs apart, depending on freestream velocity and Strouhal number, straddling two neighbouring camera frames. Phase-averaged measurements were achieved using a total of 140 image pairs taken at the same point in the oscillation. Captured images were then processed using commercially available software: TSI Insight 3G. The PIV images were processed using a recursive FFT correlator with a final interrogation window size of 16 by 16 pixels to generate a vector field of 199 $\times$ 148 vectors. This gave approximately a 1.2 mm (1.2% of the chord length) spatial resolution.

The circulation is estimated as explained in Cleaver *et al.*:[8] the vortex is located using a vortex identification algorithm with the search centred on the point of maximum absolute vorticity. The radius of the vortex is then determined by continually expanding from the centre, one spatial resolution unit at a time, until the increase in the magnitude of circulation is negative or small ($<$1%). The circulation calculation itself is done using both line integral and vorticity surface methods. The agreement between the two methods was generally very good. All circulation results presented herein are derived from the average of the two.

3. Volumetric velocimetry

Velocity measurements were also performed with a volumetric three-component velocimetry (TSI V3V) laser system. The flow was seeded with 50 μm hollow glass particles, and illuminated using a dual ND:YAG 200 mJ pulsed laser. Images were captured using three 4MP 12 bit CCD cameras, fixed within a common housing. A pair of laser cones were fired 750 μs apart, straddling two neighbouring camera frames. The positioning of the camera and the laser cone with respect to the test section is illustrated in Figure 2(b). The raw images are converted into usable results through four processing stages.

Stage 1, image-particle identification: the illuminated particles within each image are located based on user defined criteria (size, intensity etc.). Stage 2, image-particle pairing: using the location vectors from the calibration the same particles are located in each of the three images to form "triplets" that define the particles' position in 3D space. Stage 3, triplet pairing: the triplets are paired between the two times using the relaxation method first proposed by Baek and Lee[22] with a tracking group size of 8 particles, to give randomly located velocity vectors. Stage 4, grid interpolation: the randomly located vectors are interpolated onto a common grid to generate a series of uniformly spaced velocity vectors centred within voxels, 8 mm in size, with 50% overlap. The grid interpolation ultimately produced 25 000–35 000 grid vectors within a measurement volume of 152 mm $\times$ 168 mm $\times$ 136 mm. Phase-averaged measurements are based on 140 vector fields, phase-locked using the aforementioned rotary encoder. In order to capture a larger region of the flow field, a series of measurements were carried out at various spanwise locations and the different volumes merged in Matlab.

III. RESULTS AND DISCUSSION

A. Force measurements

One of the consequences of oscillating a two dimensional airfoil at sufficiently high frequency is the ability to break symmetry and develop a dual mode flow. Modes correspond to an upward

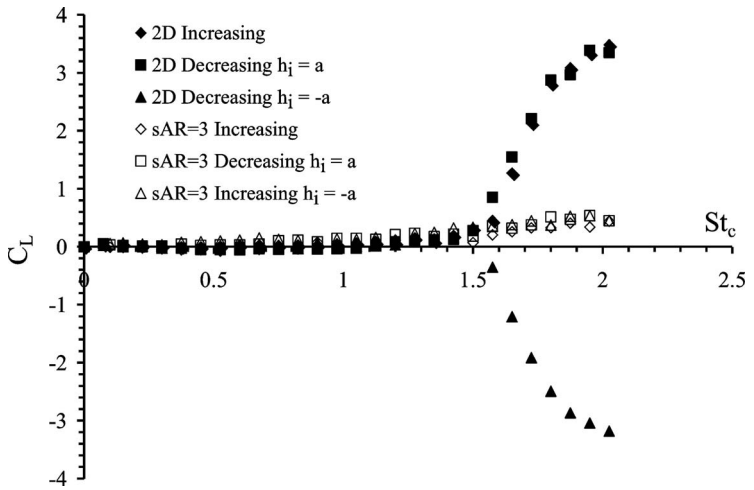

FIG. 4. A comparison of the time-averaged lift, at various operating Strouhal numbers, obtained for the effectively infinite wing (labelled 2D) and finite wing (labelled sAR = 3).

or downward deflected jet, giving rise to non-zero lift even in the case of a zero mean angle of attack. Lift coefficient measurements for an effectively infinite wing and finite wing are presented in Figure 4 for $\alpha = 0^{\circ}$, showing time-averaged lift as function of St_c. Note that in these experiments exactly the same wing and setup is used with the only difference being a tip end-plate (located at a distance $d/c = 0.02$) added to the effectively infinite wing case compared to no end-plate for the finite wing case. Force data were captured by increasing or decreasing the frequency incrementally, allowing the flow to settle after each interval. In the increasing case the wing was started from rest with an initial position of $h_i = 0$ and the first frequency being $St_c = 0.075$. In the decreasing case the wing was started from rest but with the first frequency being $St_c = 2.025$. In the decreasing case starting position has an influence[7] and so two are considered: top ($h_i = a$) or bottom ($h_i = -a$) of the motion.

The effectively infinite wing exhibits a bifurcating lift curve. The two branches develop at $St_c = 1.5$ and each corresponds to a specific mode. The upper branch corresponds to an upwards deflected jet (see Mode A in Figure 1); the lower branch corresponds to a downwards deflected jet (see Mode B in Figure 1). Which branch is produced is determined by the initial conditions, for more detail see Cleaver *et al.*[8] The relationship between the direction of the lift and deflected jet appears to be contrary to what one would intuitively expect. In the previous paper,[8] we performed a simple control-volume analysis for the typical measurement volume shown in Figure 1. This revealed that the momentum flux terms have a small contribution to the lift force. The main contribution comes from the pressure difference between the upper and lower boundaries, which can be also estimated by the Bernoulli equation.

Conversely the finite wing displays a single mode of approximately zero time-averaged lift. Therefore, the dual modes are prevented and symmetric flow is presumably preserved for the finite wing. As a result the initial condition has no effect to within the bounds of experimental uncertainty.

The only difference between the effectively infinite wing and finite wing is the addition of an end-plate near the wing tip. Therefore, to investigate the transition from single to dual modes the effect of the distance from the wing tip to this end-plate is presented in Figure 5. Proximity of the tip end-plate has the effect of inhibiting the tip vortex and thereby forcing a quasi-two-dimensional flow. Increasing the distance d allows us to gradually transition from the effectively infinite wing ($d/c = 0.02$) to the finite wing ($d/c = 1.58$, off the scale). The force measurements presented in Figure 5 represent time-averaged lift produced by the wing while oscillating at $St_c = 2.025$. The plunging motion is impulsively started from either the top ($h_i = a$) or bottom ($h_i = -a$) of the motion in order to promote the two modes. The transition from dual mode to single mode occurs over a small range of gap distances (within $0.25c$). It is also interesting to note that the variation of the

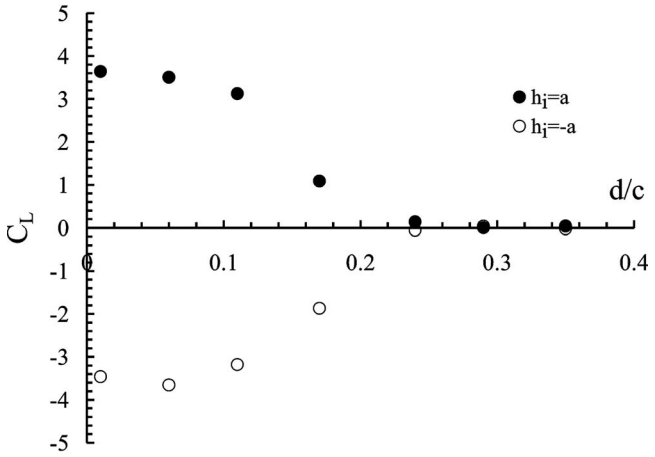

FIG. 5. The effect of varying the spacing between the wing-tip and end-plate, on the time-averaged lift generated by the $b/c = 3$ rectangular wing. The hollow and solid markers represent the wing impulsively started from the bottom and top of the motion, respectively. The wing is operating at $St_c = 2.025$ and $Re = 10\,000$.

lift force is continuous during the transition. As will be discussed later there are two contributing effects of proximity of the tip end-plate that could explain this transition: first it inhibits the tip vortex and second it creates straight vortex tubes instead of vortex rings. Both of these effects could be significant in causing the change from single to dual modes as discussed below.

B. PIV measurements

Figures 6(a) and 6(b) show time-averaged velocity magnitude for the effectively infinite wing and finite wing, respectively. The flows are for the same spanwise location (mid-span, $z/c = 1.5$). A deflected jet is produced by the effectively infinite wing, forming either side of the streamwise

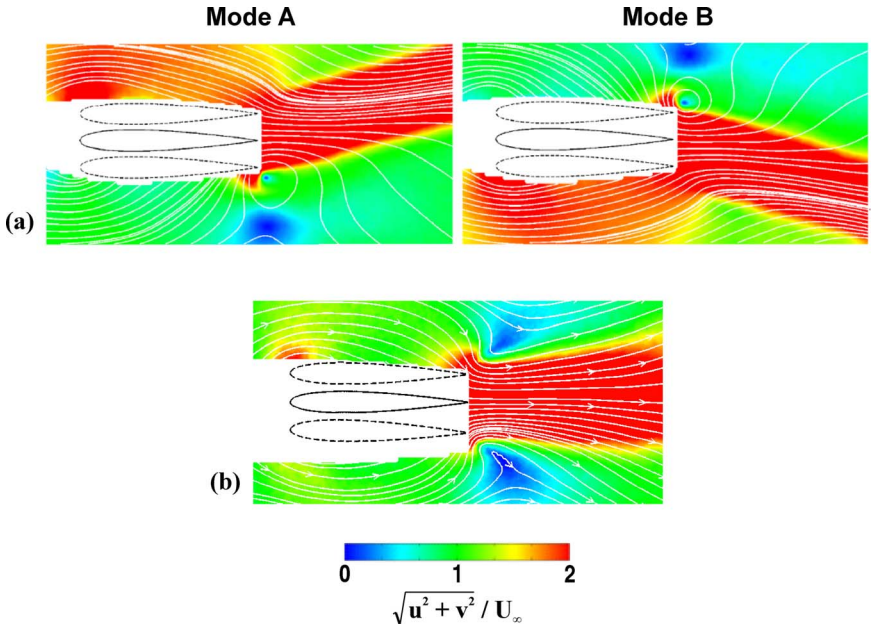

FIG. 6. Time-averaged flow showing non-dimensionalised velocity magnitude for the (a) two modes of the effectively infinite wing and (b) the symmetric flow of the finite wing, both taken at $z/c = 1.5$. The wing is oscillated with $St_c = 2.025$ at $Re = 10\,000$.

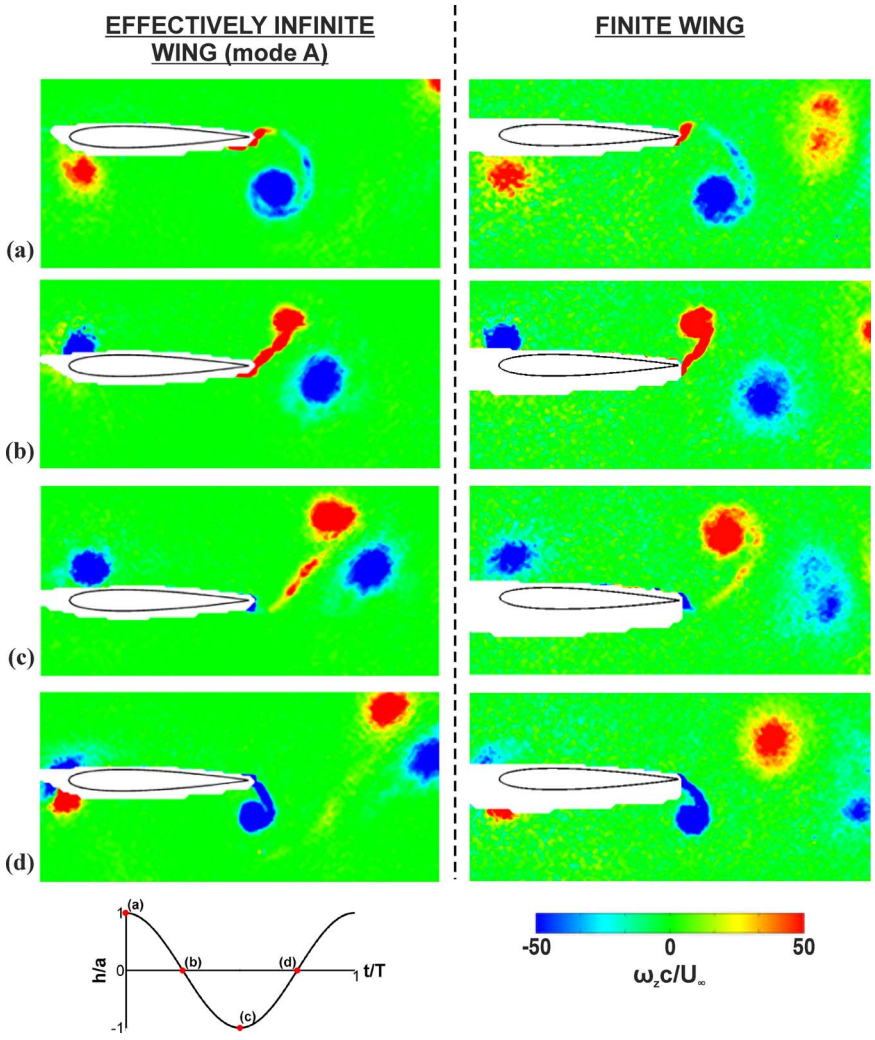

FIG. 7. Phase averaged flow showing non-dimensionalised spanwise vorticity at four phases in the cycle for the mode A flow of the effectively infinite wing (left column) and finite wing (right column), both taken at $z/c = 1.5$. The wing is oscillated with $St_c = 2.025$ at $Re = 10\,000$.

axis depending on the initial condition. A region of high velocity flow is also seen above or below the wing, depending on which of the two modes are activated. For the finite wing, symmetric flow occurs with a single jet existing approximately parallel to the streamwise flow. Moreover, the wing fails to generate a similar region of high velocity flow above or below the surface. Therefore, symmetry is preserved both downstream and upstream of the trailing edge. This agrees well with the time-averaged force measurements which indicate almost zero lift for the finite wing. Also, it is noted that, because of the relatively large aspect ratio of the finite wing (semi-aspect ratio of 3 or full aspect ratio of 6), the difference between the effectively infinite wing and finite wing is small in terms of the velocity magnitude in the wake.

Phase-averaged measurements are shown in Figure 7 in the form of spanwise vorticity for the mode-A of the effectively infinite wing and the finite wing. For the effectively infinite wing, the clockwise trailing edge vortex loiters and pairs with the counter-clockwise trailing edge vortex from the following half cycle. In this instant, the vortex pair advects above the streamwise axis, describing a "mode A" vortex pattern. For the finite wing the vortices fail to pair. Instead, the trailing edge vortices advect along the streamwise axis preserving symmetric flow. Circulation measurements of the counter-clockwise and clockwise trailing edge vortex for the finite wing indicate a strength of

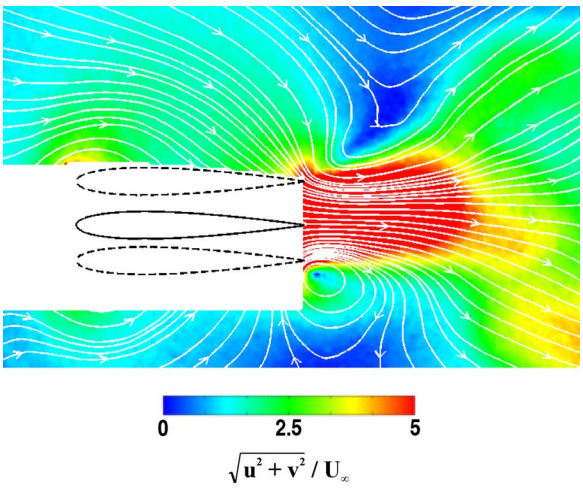

FIG. 8. Time averaged flow at the midspan plane of the finite wing, showing non-dimensionalised velocity magnitude. The wing is operating with $St_c = 4.05$ at $Re = 5000$.

$|\Gamma|/(U_\infty c) = 4.15$ and 4.16, respectively. By all three strength criteria presented in the introduction these vortices are sufficiently strong ($St_A = 0.61$, $\overline{|\Gamma|}/U_\infty c = 4.16$, $\overline{|\Gamma|}/U_{pl} c = 2.18$) to create deflected jets and dual modes. However, the asymmetry of the vortex strengths observed for deflected jets does not exist. In summary the TEVs are strong enough but balanced and therefore symmetric.

For the effectively infinite wing the asymmetry at the trailing-edge is mirrored at the leading-edge where the upper-surface LEV is stronger than the lower-surface LEV justifying the high positive lift for this case. For the finite wing, the upper and lower surface leading edge vortices have a circulation of $|\Gamma|/(U_\infty c) = 2.73$ and 2.64, respectively. The similarity in strengths for the finite wing reflects the time-averaged velocity contour as well as the near-zero time-averaged lift.

Measurements were also performed for a higher Strouhal number of $St_c = 4.05$, albeit at a lower Reynolds number of 5000, in order to investigate whether the phenomenon requires a higher excitation frequency for the finite wing. Reynolds number does not have any effect on the critical Strouhal number for bifurcation for effectively infinite wings[23] over the range of Reynolds numbers: Re = 2500–15 000. The velocity contours are presented in Figure 8. This Strouhal number is now 2.7 times greater than that where deflected jets begin for the effectively infinite wing, and despite the significantly stronger trailing edge vortices, there is no significant deflection in the wake and symmetry is still preserved. It can therefore be concluded that finite wings prevent deflected jets. Further measurements[24] for other planforms and aspect ratios demonstrate the same behaviour.

C. Volumetric velocity measurements

In Figures 9 and 10 we present vorticity iso-surfaces from a top and side view respectively. The left column is for the effectively infinite wing; the right column the finite wing. Each row represents a different phase, either: top, middle-down, bottom, or middle-up. For the effectively infinite wing the flow field is clearly asymmetric, compare Figure 9(left) with Figure 7(left). (Note that measurements were not taken near the wing root). The trailing-edge vortices are remarkably two-dimensional, forming straight vortex tubes with the only three-dimensional feature being a very small branch between the two vortices at the tip end-plate. This branch is small in comparison with the TEVs and is possibly created by the interaction of the TEV pair with the tip end-plate. There is also some vorticity generation in the small gap between the wing and the end-plate (most visible in Figures 9(b) and 10(b)). However, despite these interactions with the end-plate, the vortices in the wake are highly two-dimensional. Conversely the finite wing has a highly three-dimensional flow field. Near the root the TEVs form vortex tubes but at a spanwise location these cylinders break into a double helix structure with two branches. One branch connects with the last vortex;

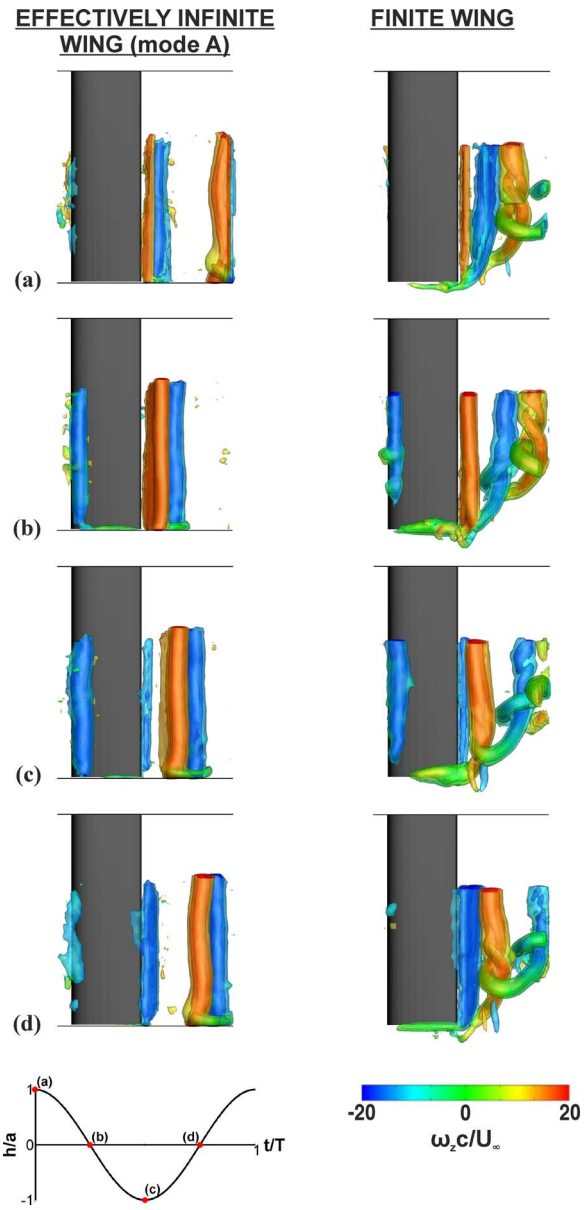

FIG. 9. Top view of iso-surfaces defined by non-dimensionalised vorticity magnitude ($\omega c/U_\infty = 14$, 25, and 50) overlaid with contours of spanwise vorticity for the effectively infinite wing (left column) and finite wing (right column). The wing is oscillated with $St_c = 2.025$ at $Re = 10\,000$.

one branch connects with the next vortex. There is therefore a long "daisy chain" of interconnected TEVs forming a long series of vortex loops. To the authors' knowledge, this is the first study that has revealed the double helix structure in the connection process of vortex loops. The point at which this double helix structure occurs moves inboard as the TEVs propagate downstream. In addition, there is a strong tip vortex.

It appears that the three-dimensionality of the trailing-edge vortices inhibit the formation of vortex couples. For the effectively infinite wing, the vortices are highly two-dimensional and form a couple. This may be a general rule with regard to the formation of vortex couples. Couder and Basdevant[25] observed the formation of vortex couples in the wakes of cylinders in two-dimensional flows generated by the soap-film technique. At the same Reynolds numbers, such vortex couples have never been observed in three-dimensional wakes. It may be that, in the present case,

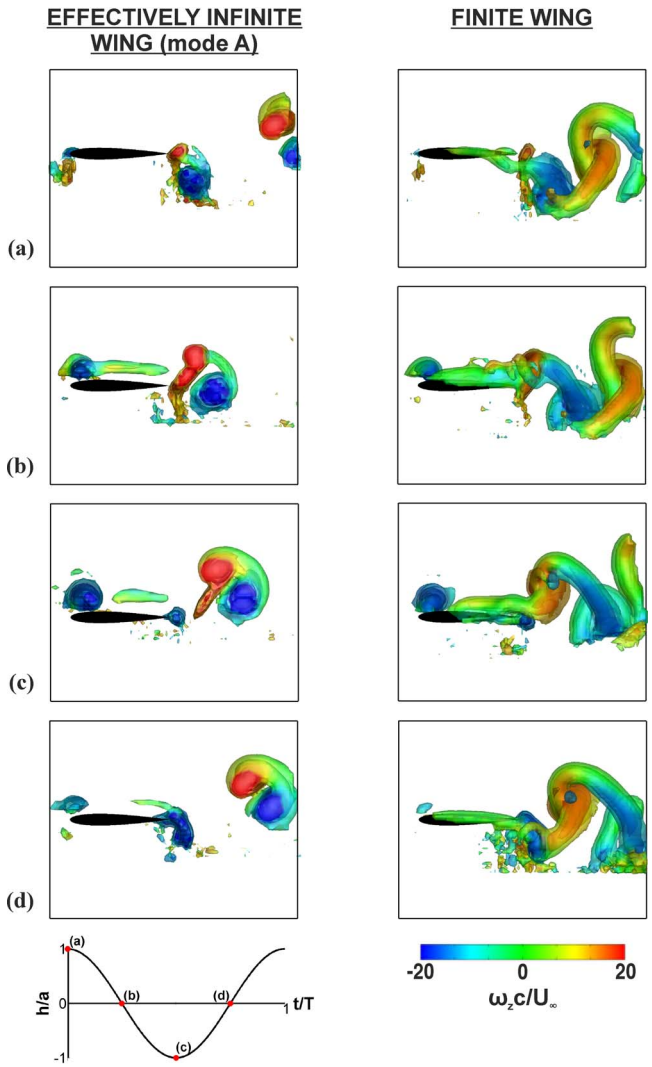

FIG. 10. Side view of iso-surfaces defined by non-dimensionalised vorticity magnitude ($\omega c/U_\infty = 14$, 25, and 50) overlaid with contours of spanwise vorticity for the effectively infinite wing (left column) and finite wing (right column). The wing is oscillated with $St_c = 2.025$ at $Re = 10\,000$.

two-dimensionality enhanced by the wing oscillations encourages the formation of a vortex couple. However, the presence of a tip vortex for the finite wing creates three-dimensionality in the vortices.

It is suggested that there are two contributing causes of the prevention of deflected jets in finite wing cases: the tip vortex and vortex loops. The tip vortex is generated around the same time as the newest trailing-edge vortex, and these are topologically connected. Tip vortices of opposite sign form at the locations that are mirror images of each other. Hence there is symmetry (with respect to the free stream direction) in the formation of the tip vortices. We believe that, as the tip vortices are connected to the trailing-edge vortices, this discourages the formation of vortex coupling, which of course results in asymmetry with respect to the freestream direction. Another effect of the tip vortex is the upwash or downwash velocity induced on the spanwise vortices. For example, downwash created in Phase (b) (in Figures 7 and 9) may produce an adverse strain, which may encourage separate vortices.[26] The second contributing factor is the vortex loops in the wake. One of the central observations made by Cleaver *et al.*[8] for the effectively infinite wing is that the direction of deflected jets is characterized by asymmetry in the TEV strength which is defined by the asymmetry parameter. This asymmetry in TEV strength was observed for all dual mode cases studied. For the

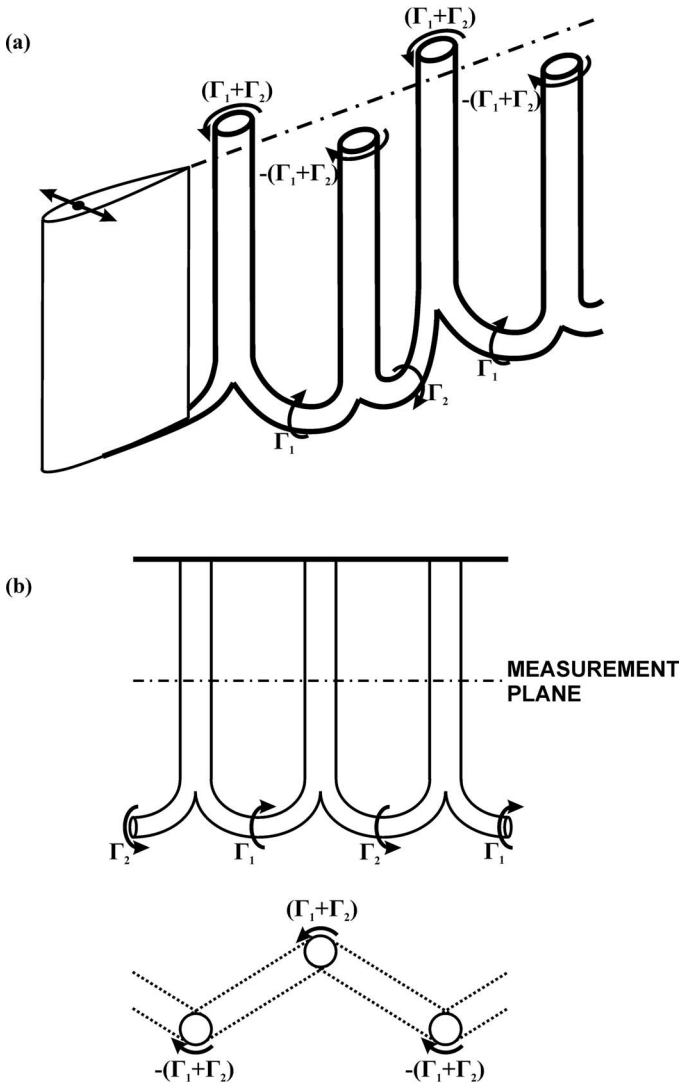

FIG. 11. (a) Simplified isometric view of the vortex chain and (b) top and side view.

vortex loops observed in Figures 9 and 10 this asymmetry cannot be supported. In Figure 11 we show a simplified schematic of the vortex loop system (for clarity we omit the details such as the double helix structure and vortex formation process). In addition to the isometric view, we show two other views, a top view from above the vortex loops and a side view of the section plane shown with a dashed line in the top view. In this side view, the conventional inverse Karman vortex street is observed. The loops of opposite sign have the absolute circulations of Γ_1 and Γ_2, and in the streamwise plane the total circulations are $(\Gamma_1+\Gamma_2)$ and $-(\Gamma_1+\Gamma_2)$. Hence, regardless of whether the loops have the same circulation ($\Gamma_1 = \Gamma_2$) or differing circulation ($\Gamma_1 \neq \Gamma_2$) the total circulation of the trailing-edge vortices, that are crucial for asymmetric wakes, will always remain equal. Indeed we have measured the total circulation and found equal magnitudes ($|\Gamma|/U_\infty c = 4.15$ and 4.16). Therefore, the symmetry (in terms of magnitude of the circulation analogous to the two-dimensional case) is a natural consequence of the interconnected vortex loops for the finite wing case.

IV. CONCLUSIONS

Force, PIV, and Volumetric Velocimetry measurements have been presented which show that finite wings inhibit deflected jets. The transition from dual-mode high-lift deflected jets to single-

mode near zero-lift flow fields was shown to occur as the distance of the end-plate from the tip is varied. A tip spacing of just $0.25c$ was sufficient to enforce a single-mode flow field. In the effectively infinite wing case the trailing-edge vortices form straight vortex tubes that pair and convect at an angle to the horizontal creating asymmetry as previously reported by other authors. With the tip end-plate removed to create a finite wing the flow field becomes highly three-dimensional. Near the root the TEVs form straight vortex tubes but at a spanwise location these cylinders break into a double helix structure with two branches. One branch connects with the last vortex; one branch connects with the next vortex. There is therefore a long "daisy chain" of interconnected TEVs forming a long series of vortex loops. In addition, there is also now a strong tip vortex. It is suggested that there are two contributing reasons for this abrupt change. First the tip vortex creates three-dimensionality that prevents vortex coupling. It is noted that there is other evidence of formation of vortex couples in two-dimensional flows and absence of vortex couples when there is some three-dimensionality. Second, the circulation of the interconnected vortex loops is symmetric due to the vortex topology of finite wing, and this is confirmed by the circulation measurements. Therefore the asymmetry previously observed as characteristic of deflected jets cannot be supported for finite wings.

ACKNOWLEDGMENTS

The work was sponsored by the Air Force Office of Scientific Research, Air Force Material Command, USAF under Grant No. FA8655-10-1-3093, as well as the Engineering and Physical Sciences Research Council (EPSRC) Studentship, and the RCUK Academic Fellowship in Unmanned Air Vehicles.

[1] I. Gursul, D. J. Cleaver, and Z. Wang, "Control of low Reynolds number flows by means of fluid-structure interactions," Prog. Aerosp. Sci. **64**, 17–55 (2014).
[2] J. D. Elldredge and K. Chong, "Fluid transport and coherent structures of translating and flapping wings," Chaos **20**(1), 017509 (2010).
[3] M. M. Koochesfahani, "Vortical patterns in the wake of an oscillating airfoil," AIAA J. **27**, 1200–1205 (1989).
[4] J. B. Bratt, *Flow patterns in the wake of an oscillating airfoil* (Aeronautical Research Council, London, UK, 1950), Report No. R & M 2773.
[5] K. D. Jones, C. M. Dohring, and M. F. Platzer, "Experimental and computational investigation of the Knoller-Betz effect," AIAA J. **36**(7), 1240–1246 (1998).
[6] R. Godoy-Diana, J. L. Aider, and J. E. Wesfreid, "Transitions in the wake of a flapping foil," Phys. Rev. E **77**(1), 016308 (2008).
[7] C. L. Liang, K. Ou, S. Premasuthan, A. Jameson, and Z. J. Wang, "High-order accurate simulations of unsteady flow past plunging and pitching airfoils," Comput. Fluids **40**(1), 236–248 (2011).
[8] D. J. Cleaver, Z. Wang, and I. Gursul, "Bifurcating flows of plunging airfoils at high Strouhal umbers," J. Fluid Mech. **708**, 349–376 (2012).
[9] G. C. Lewin and H. Haj-Hariri, "Modelling thrust generation of a two-dimensional heaving airfoil in a viscous flow," J. Fluid Mech. **492**, 339–362 (2003).
[10] S. Heathcote and I. Gursul, "Jet switching phenomenon for a periodically plunging airfoil," Phys. Fluids **19**(2), 027104 (2007).
[11] D. J. Cleaver, Z. Wang, and I. Gursul, "Investigation of mechanisms of high lift for a flat-plate airfoil undergoing small-amplitude plunging oscillations," AIAA J. **51**(4), 968 (2013).
[12] J. E. Emblemsvag, R. Suzuki, and G. Candler, "Numerical simulation of flapping micro air vehicles," AIAA Paper No. 2002-3197, 2002.
[13] K. D. von Ellenrieder and S. Pothos, "PIV measurements of the asymmetric wake of a two dimensional heaving hydrofoil," Exp. Fluids **44**(5), 733–745 (2008).
[14] R. Godoy-Diana, C. Marais, J. L. Aider, and J. E. Wesfreid, "A model for the symmetry breaking of the reverse Benard-von Karman vortex street produced by a flapping foil," J. Fluid Mech. **622**, 23–32 (2009).
[15] M. L. Yu, H. Hu, and Z. J. Wang, "Experimental and numerical investigations of the asymmetric wake vortex structures around an oscillating airfoil," AIAA Paper No. 2012-0299, 2012.
[16] K. D. von Ellenrieder, K. Parker, and J. Soria, "Flow structures behind a heaving and pitching finite-span wing," J. Fluid Mech. **490**, 129–138 (2003).
[17] P. Blondeaux, F. Fornarelli, L. Guglielmini, M. S. Triantafyllou, and R. Verzicco, "Numerical experiments on flapping foils mimicking fish-like locomotion," Phys. Fluids **17**(11), 113601 (2005).
[18] K. Parker, K. D. von Ellenrieder, and J. Soria, "Using stereo multigrid DPIV (SMDPIV) measurements to investigate the vortical skeleton behind a finite-span flapping wing," Exp. Fluids **39**(2), 281–298 (2005).
[19] K. Parker, K. D. von Ellenrieder, and J. Soria, "Morphology of the forced oscillatory flow past a finite-span wing at low Reynolds number," J. Fluid Mech. **571**, 327–357 (2007).

[20] H. Dong, R. Mittal, and F. M. Najjar, "Wake topology and hydrodynamic performance of low-aspect-ratio flapping foils," J. Fluid Mech. **566**, 309–343 (2006).
[21] J. H. J. Buchholz and A. J. Smits, "On the evolution of the wake structure produced by a low-aspect-ratio pitching panel," J. Fluid Mech. **546**, 433–443 (2006).
[22] S. J. Baek and S. J. Lee, "A new two-frame particle tracking algorithm using match probability," Exp. Fluids **22**(1), 23–32 (1996).
[23] D. J. Cleaver, "Low Reynolds number flow control through small-amplitude high-frequency motion," Ph.D. thesis (University of Bath, 2011).
[24] D. E. Calderon, D. J. Cleaver, Z. Wang, and I. Gursul, "Wake structure of plunging finite wings," AIAA 2013-2993, 2013.
[25] Y. Couder and C. Basdevant, "Experimental and numerical study of vortex couples in two-dimensional flows," J. Fluid Mech. **173**, 225 (1986).
[26] R. R. Trieling, J. M. A. van Wesenbeeck, and G. J. F. van Heijst, "Dipolar vortices in a strain flow," Phys. Fluids **10**(1), 144 (1998).